Project Title: Prediction, Sensitivity, and Dynamics of Subseasonal To Seasonal Phenomena Diagnosed Through Linear Inverse Models, Their Adjoints, and Numerical Weather Prediction Models
PI(s): Brett T. Hoover (University of Wisconsin – Madison, SSEC/CIMSS), Matt Newman (University of Colorado – Boulder, PSD, CIRES), Daniel J. Vimont (University of Wisconsin – Madison), Michael C. Morgan (University of Wisconsin – Madison)
Major contributors: Melissa Breeden (University of Wisconsin – Madison)

1. Focus

The focus of our project was on the subseasonal prediction of North Pacific blocking events, which represent a low-frequency weather extreme with large impacts both up- and downstream and is recognized as a significant forecast challenge for subseasonal numerical weather prediction (NWP). The project addressed several key questions of the MAPP S2S Project, cutting across the "Processes and Physics" and "Approaches to S2S Prediction" focus areas. The key questions in Processes and Physics being addressed are:

- What are the dominant physical sources of S2S predictability, and how well are these sources simulated and predicted?
- How do tropical/extra-tropical and stratosphere/troposphere connections influence S2S prediction?

The key question in Approaches to S2S Prediction being addressed is:

- What indices/metrics best describe extreme weather phenomena relevant to S2S prediction given the limitations in available model and observed variables?

2. Introduction

We approached this problem using dimension reduction and empirical modeling techniques wherein the physics that drive the evolution of blocking in the North Pacific are statistically inferred from the leading empirical orthogonal functions (EOFs) of a small subset of reanalysis variables. In our case, the physics that drive North Pacific blocking are inferred from three variables: northern hemispheric 850 hPa streamfunction, northern hemispheric 200 hPa streamfunction – which represent lower- and upper-tropospheric dynamics, mostly in the midlatitudes, and tropical outgoing longwave radiation flux (OLR) – representing midlatitude dynamics, tropical convection, and their interactions. These variables are time-averaged within a 5-day moving boxcar with the climatological mean removed. This produces our state variable:

$$\mathbf{x} = \begin{bmatrix} \psi_{200} \\ \psi_{850} \\ OLR \end{bmatrix} \quad (1),$$

and 30 years of state variable data is used to define a propagator-matrix $\mathbf{G}$ that evolves $\mathbf{x}$ from time t to $t + \Delta t$:

$$\mathbf{x}_{t+\Delta t} = \mathbf{G}\mathbf{x}_t \quad (2).$$

The propagator $\mathbf{G}$ is either defined for the subseasonal forecast range of interest directly (i.e. Markov Modeling) or is defined for a shorter range that is then applied in an log-linear framework

to produce forecasts at the desired subseasonal range (i.e. Linear Inverse Modeling). In Linear Inverse Modeling, the linear inverse model (the LIM) is computed from the covariance matrix of $\mathbf{x}$ at lags of 0 ($\mathbf{C}_0$) and τ days ($\mathbf{C}_\tau$):

$$\mathbf{L} = ln\left(\mathbf{C}_\tau \mathbf{C}_0^{-1}\right)/\tau \quad (3).$$

A forecast is produced by assuming that the relationship defined by $\mathbf{L}$ is extensible to longer forecast lead-times by linearly scaling $\mathbf{L}$ by the desired forecast length, Δt:

$$\mathbf{x}(t_0 + \Delta t) = e^{\mathbf{L}\Delta t}\,\mathbf{x}(t_0) \quad (4).$$

It is clear from Equation 2 that $e^{\mathbf{L}\Delta t} \sim \mathbf{G}$ in linear inverse modeling. The covariance lag τ is typically 7 days for our model. A LIM produced from 2-degree resolution global data from the National Center for Atmospheric Research (NCAR) Climate Forecast System Reanalysis (CFSR) performs better than a persistence model or an autoregressive model with a 1-day lag when evaluated against an L2 norm (Fig. 1).
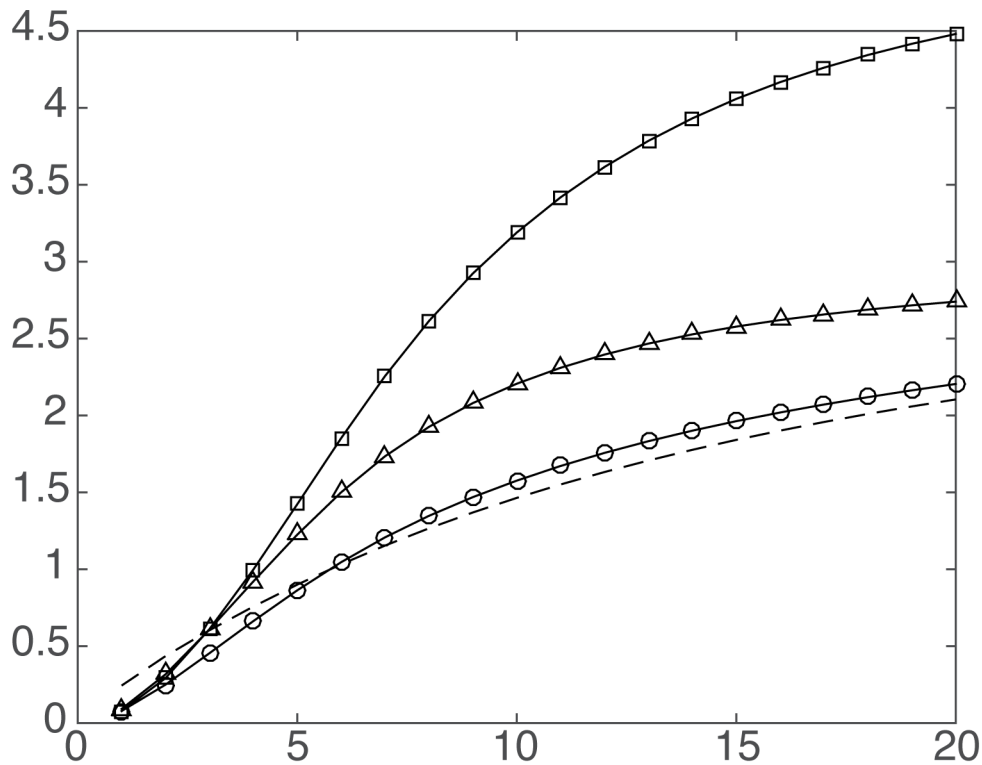
Figure 1. Forecast errors for lags from 1-20 days from the LIM (circles), a 1-day-lag autoregressive model (triangles), and a bare persistence forecast (squares). The dashed line represents the theoretically defined expectation of the LIM error.

Since our interest is in modeling blocking, we produced a Pacific blocking norm by compositing historical Pacific blocking events and projecting the composite into the LIM's EOF subspace, retaining only the ψ_{200} and ψ_{850} components (Fig. 2).
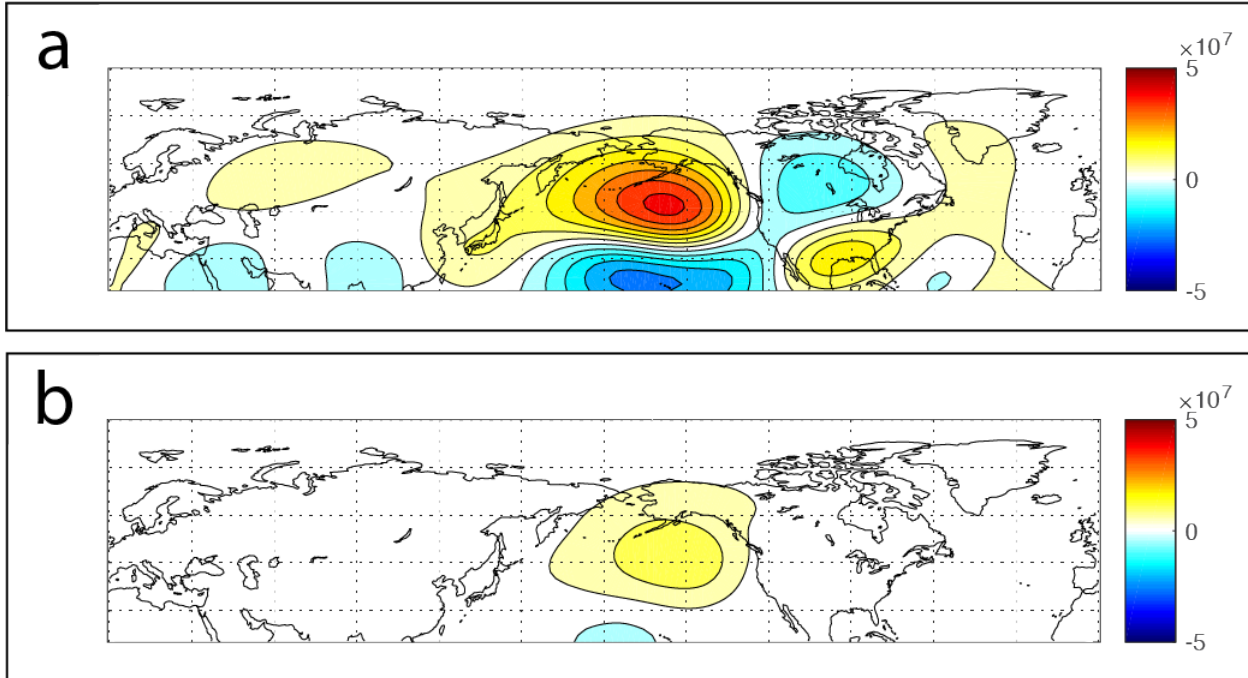
Figure 2. Blocking norm projected into EOF subspace of LIM. (a) Anomalous 7-day averaged 200 hPa streamfunction. (b) Anomalous 7-day averaged 850 hPa streamfunction.

The blocking norm in EOF space, denoted by $\mathbf{N}$, is used to derive optimal initial conditions that grow in the direction of Pacific blocking. For a chosen lead-time Δt, the leading eigenvector of $\mathbf{G^T N N^T G}$ defines the optimal initial conditions to maximize growth in the direction defined by $\mathbf{N}$. The computation of this optimal and examination of its structure is central to research into subseasonal blocking dynamics and prediction performed in this study.

3. Blocking Dynamics

The optimal initial conditions to grow a block based on the Pacific blocking norm is computed in the a-LIM for a 15-day forecast period (Fig.3).
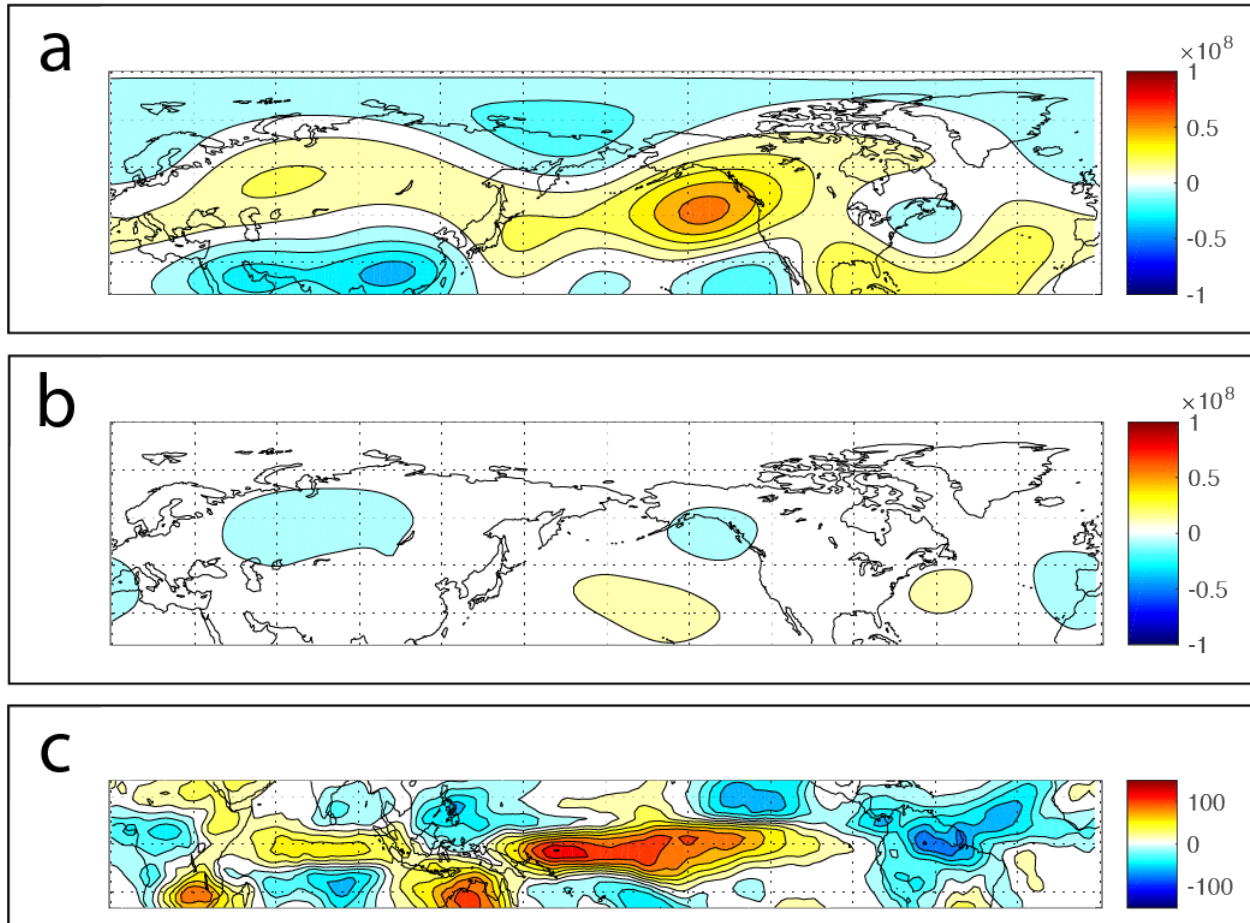
Figure 3. Optimal initial conditions to grow a block in the a-LIM for a 15-day forecast period. (a) Anomalous 7-day averaged 200 hPa stream function. (b) Anomalous 7-day averaged 850 hPa stream function. (c) Anomalous 7-day averaged tropical OLR.

The optimal conditions to grow a block by day-15 as defined by the blocking norm includes a 200 hPa anticyclone over the coast of British Columbia and significant baroclinicity resulting in a low-amplitude oppositely-signed anomalous flow at 850 hPa.

When evolved in the a-LIM for a 15-day forecast, the model produces a strong Pacific block (Fig. 4). The anticyclone at 200 hPa appears to retrograde westward and amplify over the 15-day period, producing a strong Pacific block at 200 hPa projecting strongly onto the PNA, and a broad anticyclone at 850 hPa. The tropical OLR in the equatorial tropics has characteristics of ENSO variability in the central Pacific and MJO variability in the Indian Ocean.
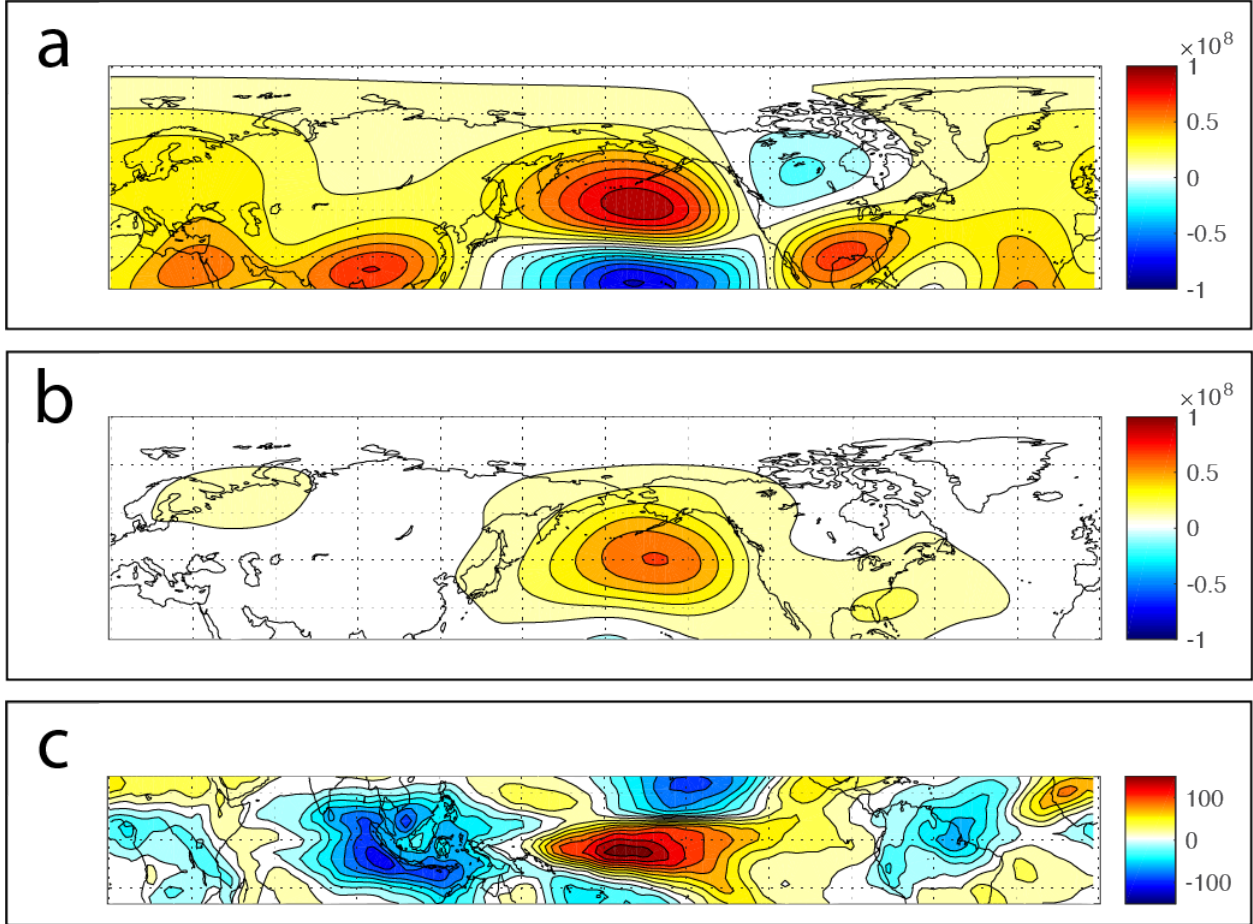
Figure 4. LIM day-15 forecast state from optimal initial conditions. (a) Anomalous 7-day averaged 200 hPa stream function. (b) Anomalous 7-day averaged 850 hPa stream function. (c) Anomalous 7-day averaged tropical OLR.

Growth in the direction of $\mathbf{N}$ from t to $t + \Delta t$ is defined by:

$$growth = \frac{\mathbf{x}(t+\Delta t)^\mathrm{T}\mathbf{N}\mathbf{x}(t+\Delta t)}{\mathbf{x}(t)^\mathrm{T}\mathbf{D}\mathbf{x}(t)} \qquad (5),$$

where $\mathbf{D}$ defines an initial norm; in this case the initial norm is chosen as the L2 norm and $\mathbf{D}$ is an identity matrix. The amount of possible growth computed as an amplification factor shows that maximum blocking growth appears at forecasts of 10 days, and positive growth is possible as far out as 28 days (Fig. 5).
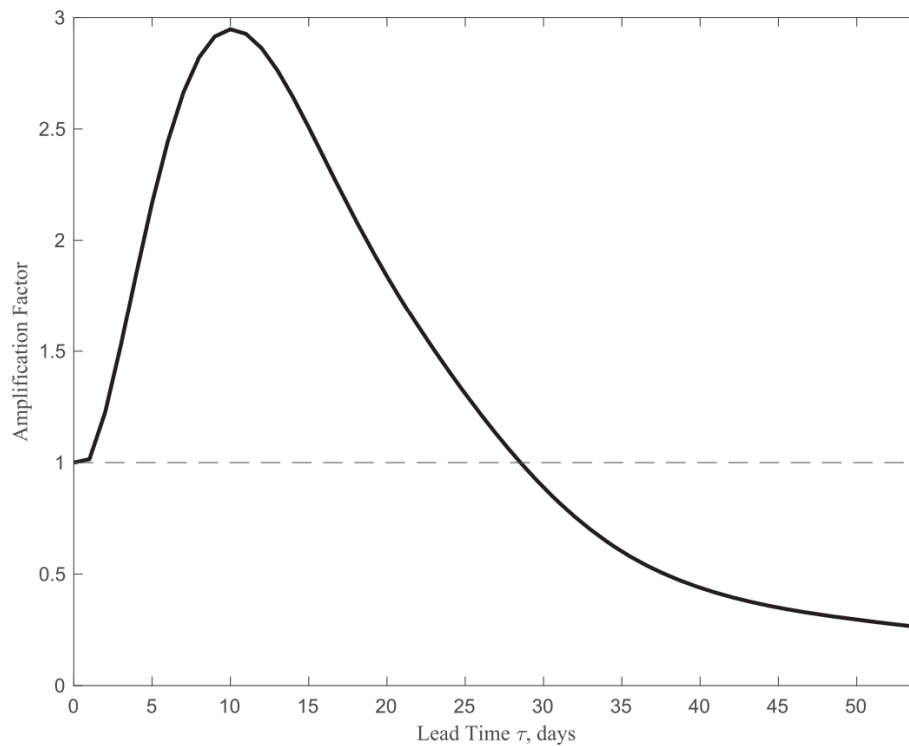
Figure 5. Maximum system growth in the LIM, as defined by the blocking norm, as a function of lead time. Adapted from Figure 7 of Breeden et al. (2020)

For a lead time of 14 days, the optimal initial conditions for blocking growth are similar in form to those of Figure 3, with an anticyclonic anomaly at 200 hPa off the coast of British Columbia and OLR growth over 14 days that implies both ENSO and MJO evolution (Fig. 6). The optimal initial condition is separated into the streamfunction (ψ_{200} and ψ_{850}) and OLR components, and the LIM is initialized with each component individually to evolve the state 14 days, in order to evaluate the relative contribution of both components (midlatitude dynamics and tropical convection). For a lead time of 14 days, the majority of the blocking growth can be attributed to the streamfunction component of the optimal initial state, though the OLR component of the optimal initial state contributes a not-insignificant portion as well as driving much of the OLR evolution (Fig. 7).

When evaluating the contribution of blocking amplitude in the LIM forecast over a range of forecast lead times, a clear pattern emerges; as the forecast lead time increases, the OLR component of the optimal initial conditions contributes a larger portion to the total blocking growth (Fig. 8), and at a 21-day lead time the blocking is contributed to equally by the streamfunction and OLR components of the optimal initial conditions.
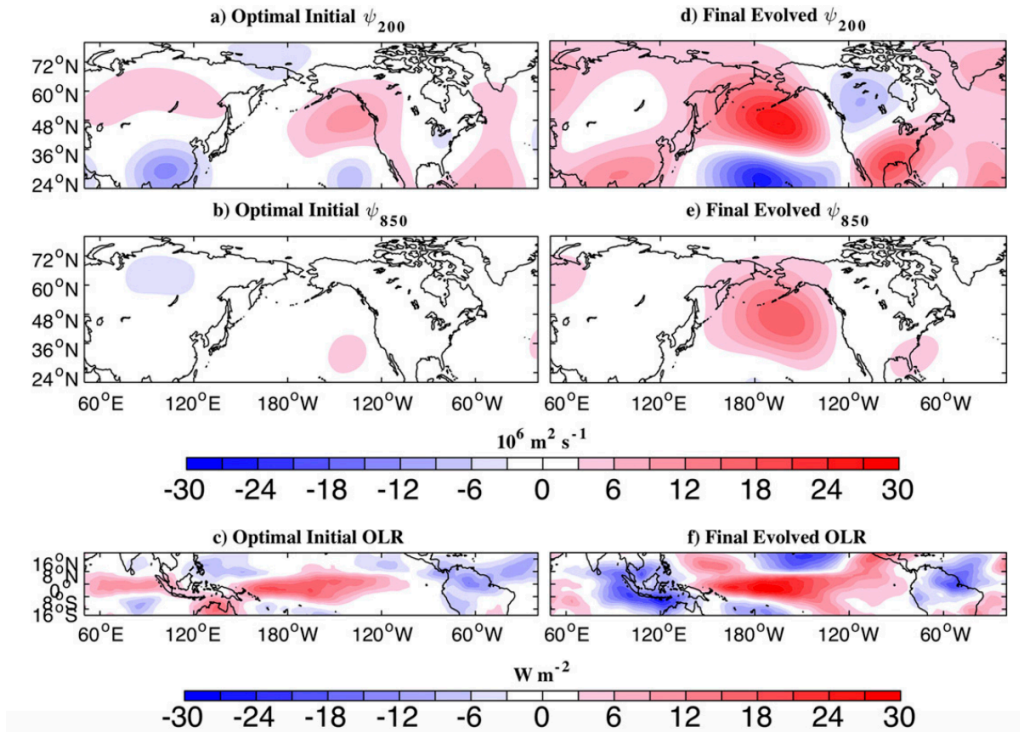
Figure 6. Optimal initial conditions for blocking growth with a lead time of 14 days, with evolved state after 14 days in the LIM. Adapted from Figure 8 of Breeden et al. (2020).
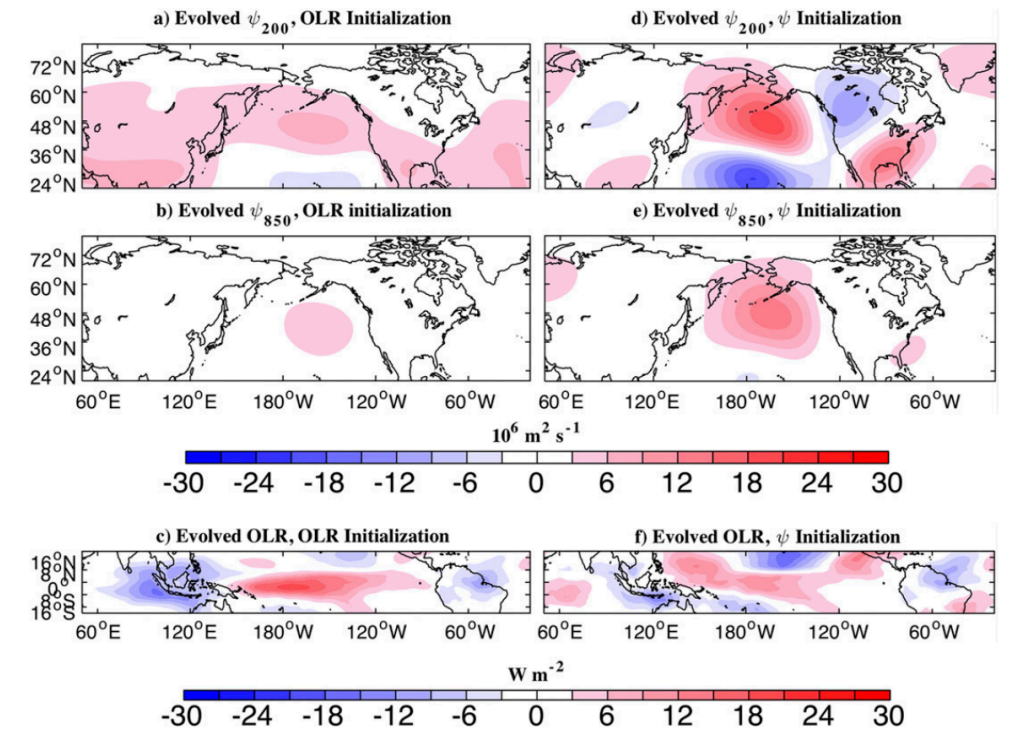
Figure 7. The 14 day evolved state in the LIM from initializing with (panels a-c) only the OLR component of the optimal initial state, and (panels d-f) only the 850 hPa and 200 hPa streamfunction component of the optimal initial state. Adapted from Figure 10 of Breeden et al. (2020).
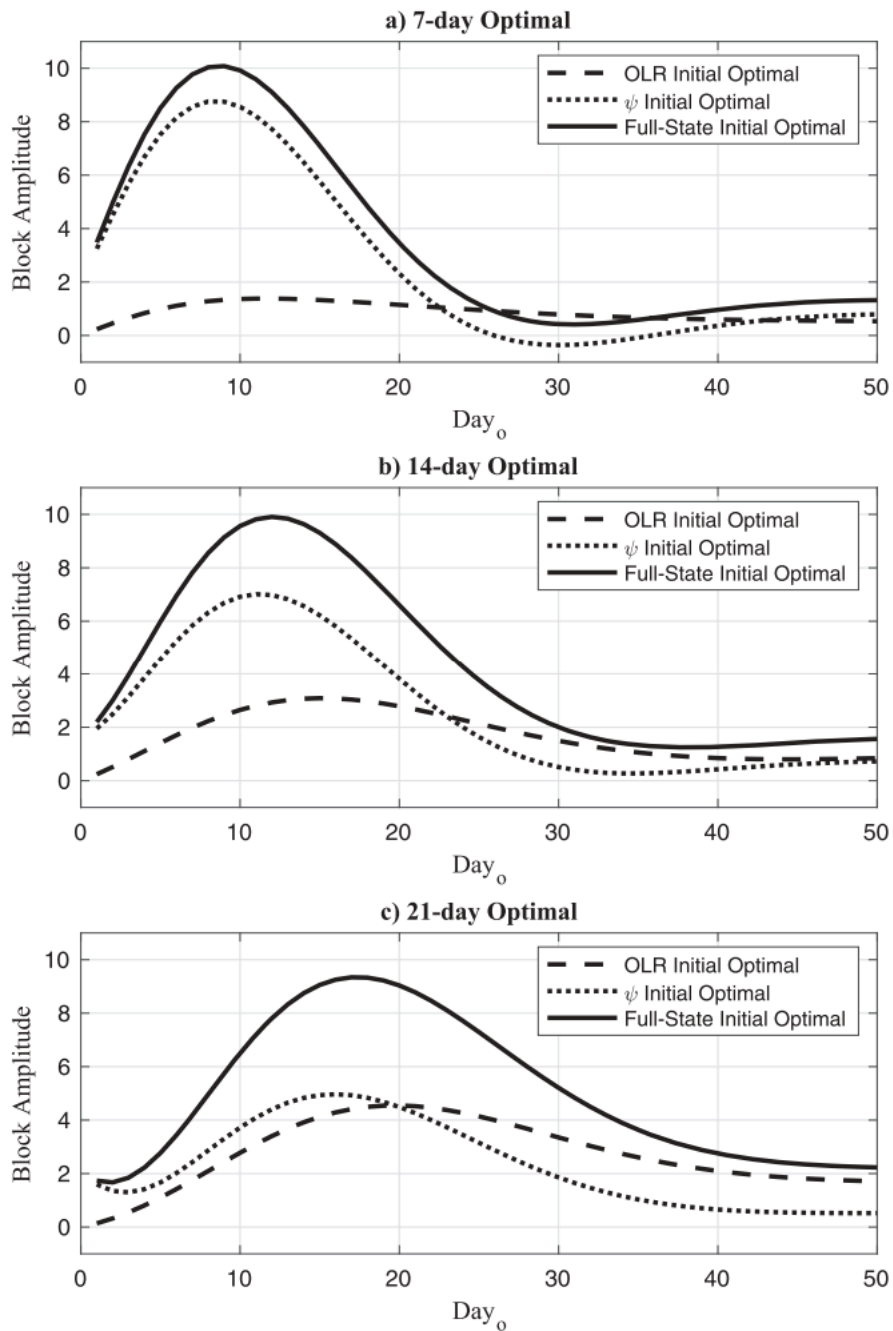
Figure 8. Block amplitude in the model as a function of forecast lead time for the entire optimal initial condition, the OLR component only, and the streamfunction component only, for (a) a 7-day optimization time, (b) a 14-day optimization time, and (c) a 21-day optimization time. Adapted from Figure 13 of Breeden et al. (2020).

4. Blocking Prediction

A core component of our proposed research was focused on using the LIM to evaluate the deficiencies of numerical weather prediction (NWP) of blocking events at subseasonal timescales.

This is accomplished through Markov models (computing $\mathbf{G}$) or LIMs (computing $\mathbf{L}$) trained on lagged covariance of $\mathbf{x}$ in the model forecast rather than in lagged analysis. The Markov model or LIM produced from the forecast covariance was anticipated to retain an empirically derived representation of the physics driving the model, which can be directly compared to the physics driving the real evolution of the atmosphere in the low-dimensional space of the Markov model/LIM. The blocking prediction of the LIM depends on the strength of the relationship between the projection of the initial state onto the optimal initial conditions and the projection of the final state onto the blocking norm – how predictive is the optimal initial conditions in predicting a block? How often does a state that projects strongly onto the optimal initial conditions produce a block within the prescribed forecast lead time?

We produced two LIMs from 30 years of Global Ensemble Forecast System (GEFS) reanalysis/reforecast data – an analysis-based LIM (a-LIM) computed from time-lagged analyses and a forecast-based LIM (f-LIM) computed from the covariance between the analysis and GEFS (control) forecast. A direct comparison of LIM components shows there are global differences in physics driving the two models (Fig. 9).
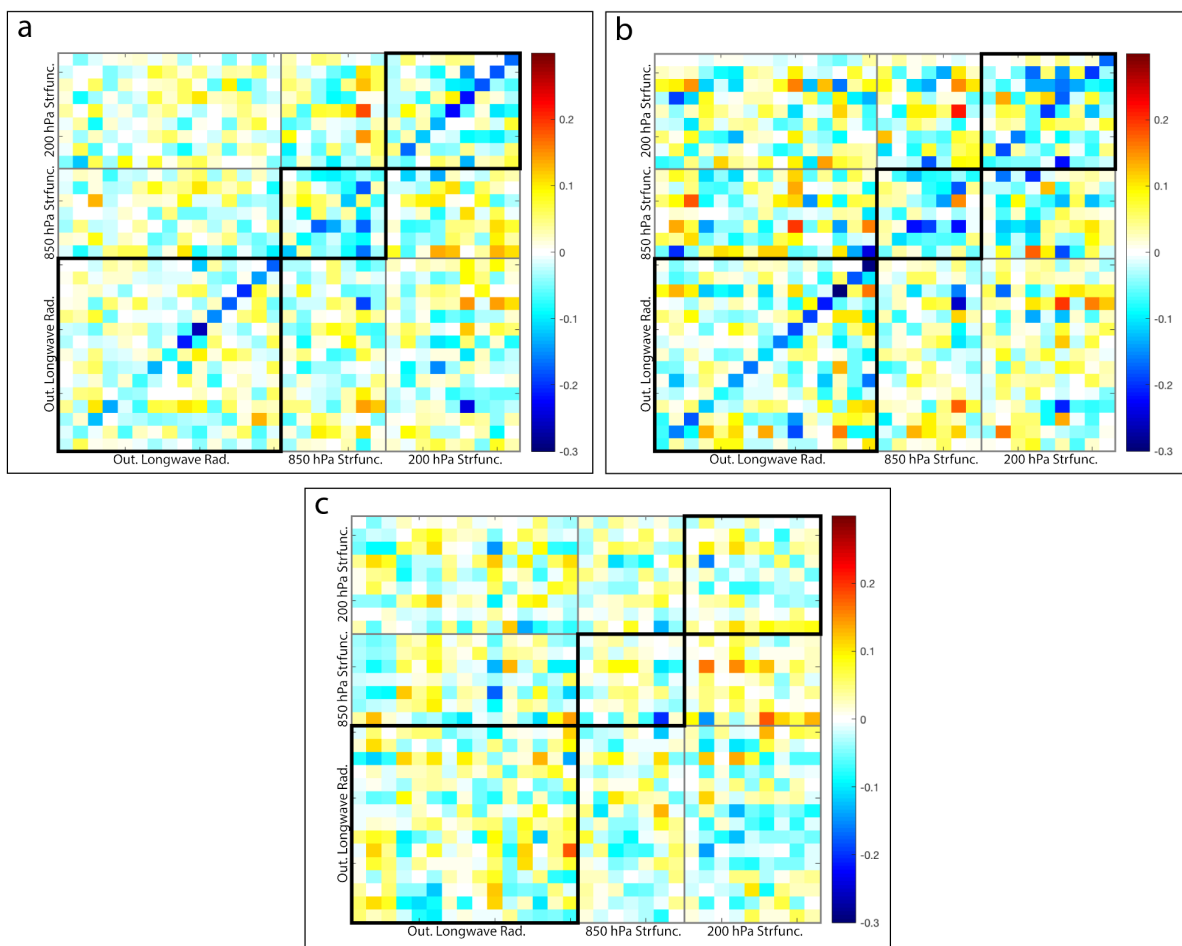
Figure 9. LIM $\mathbf{L}$-matrix components of the (a) a-LIM, and (b) f-LIM. The differences (a-LIM minus f-LIM) is provided in panel c.

The optimal initial condition for growing blocks in

A blocking-index is produced for the analysis and the 21-day LIM forecast as a normalized projection onto the blocking norm. While several blocked events in the verification are missed by both the a-LIM and f-LIM forecast, the prolonged periods of negative index (indicating large-scale cyclonic flow in the north Pacific) are well forecast (Fig. 10).
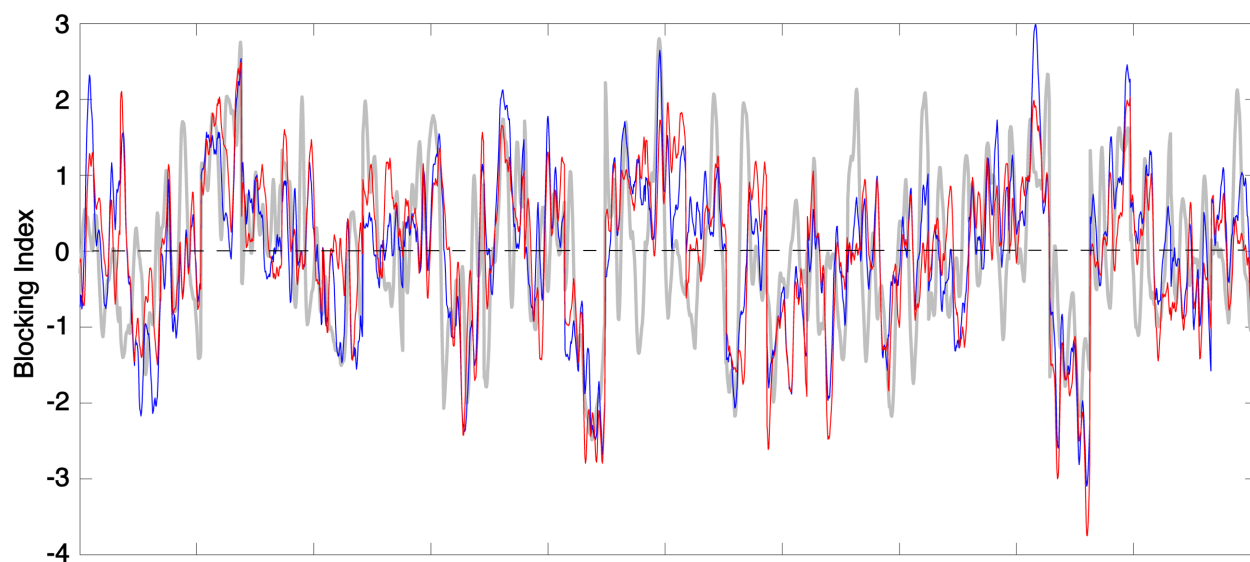
Figure 10. Blocking index over 30-year dataset. Verification is in gray, a-LIM 21-day forecast is in blue, and f-LIM 21-day forecast is in red.

In a scatter-plot, the a-LIM demonstrates greater skill in forecasting blocks than the f-LIM, with the 95% confidence ellipse of the covariance between the forecast and verification adhering closer to the y=x (perfect forecast) line (Fig. 11). The correlation of the 21-day forecast to verification is r=0.53 in the a-LIM and r=0.46 in the f-LIM. The optimal initial conditions in the f-LIM for blocking drives amplification that is larger than that of the optimal initial conditions in the a-LIM for lead times in the first 2 weeks of the forecast, but in the second 2 weeks the f-LIM is deficient in growing blocks (Fig. 12).

The impact of manipulating parts of the f-LIM **L**-matrix on blocking growth is explored with two techniques: (1) a regression map computed from random perturbation of the elements of the **L**-matrix, and (2) a map computed from replacing elements one-by-one of the f-LIM with corresponding elements of the a-LIM (Fig. 13). In both cases, there are significant sensitivities of blocking to elements of the f-LIM's **L**-matrix that take the form of vertical columns, representing the impact of one EOF on the entire system. When five of these columns are selected (two representing the system-wide interaction of OLR EOFs and three representing the system-wide interaction of 200 hPa streamfunction EOFs) and replaced with corresponding columns of the a-LIM, blocking growth in the modified f-LIM is greatly enhanced at 21 days (Fig. 14).
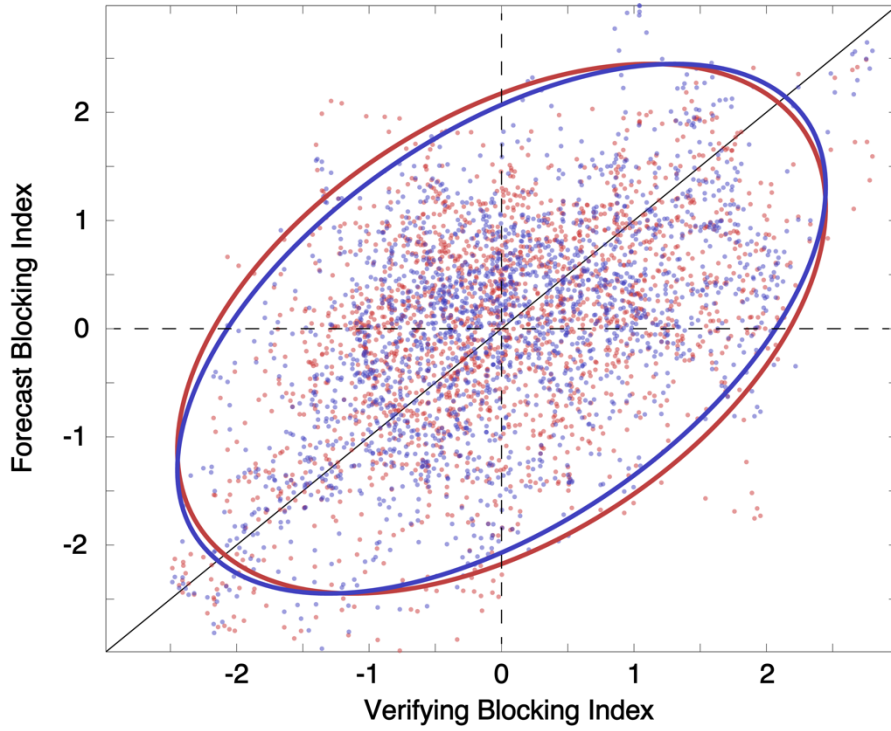
Figure 11. Scatter plot of projection of verifying day-21 analysis onto blocking norm versus the projection of the 21-day a-LIM forecast (blue) and f-LIM forecast (red) onto the blocking norm. Projections are normalized, with a perfect forecast falling along the black line. The blue (red) ellipse represents the 95% bounds of the covariance for the a-LIM (f-LIM) forecast against the verification.
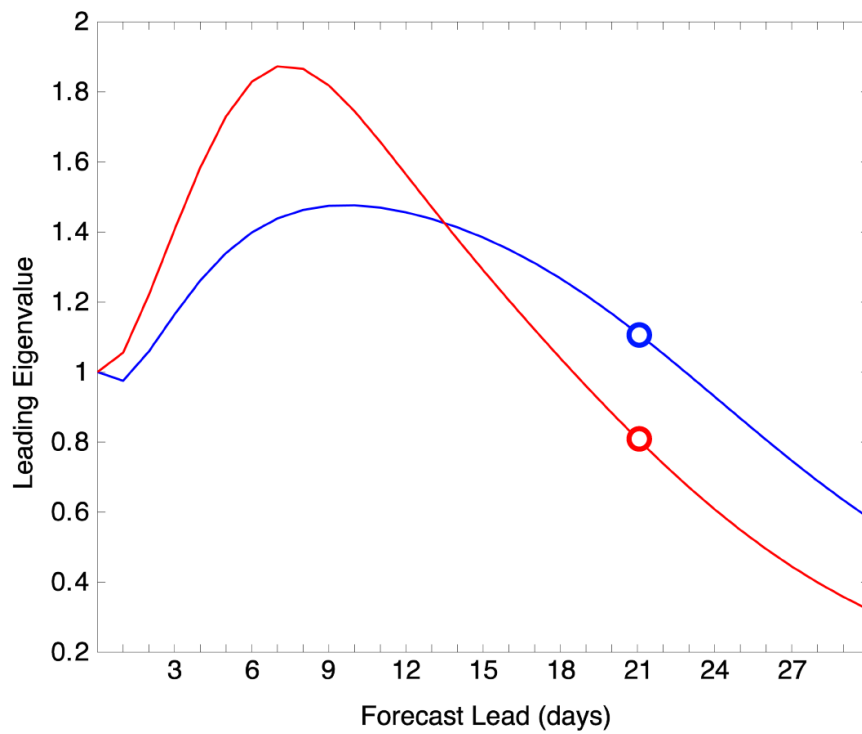
Figure 12. Amplification factor of blocking growth in the a-LIM (blue) and f-LIM (red) as a function of forecast lead time. The circles highlight values at 21-days.
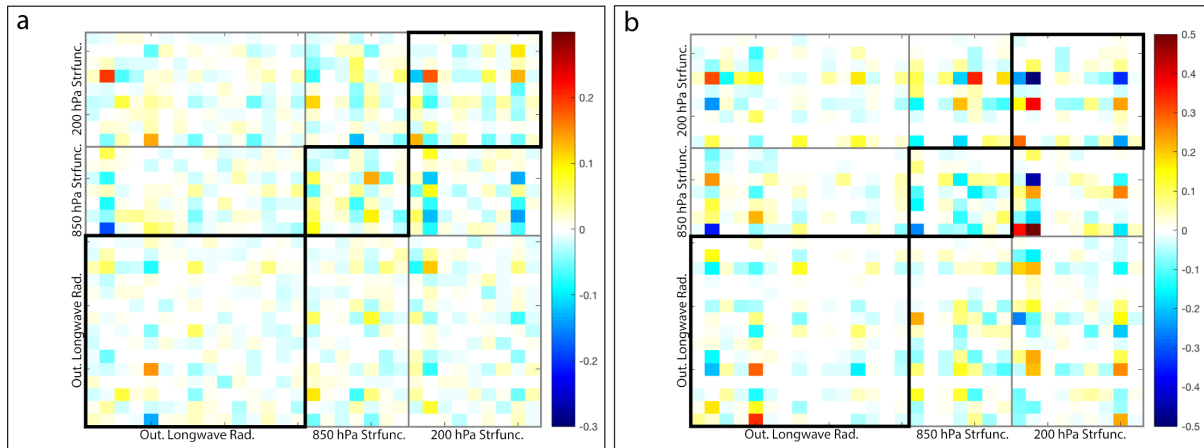
Figure 13. Sensitivity of 21-day blocking in the f-LIM to elements of the **L**-matrix via (a) regression map based on random perturbation of the **L**-matrix, and (b) element-by-element replacement of the f-LIM **L**-matrix components with corresponding a-LIM components.
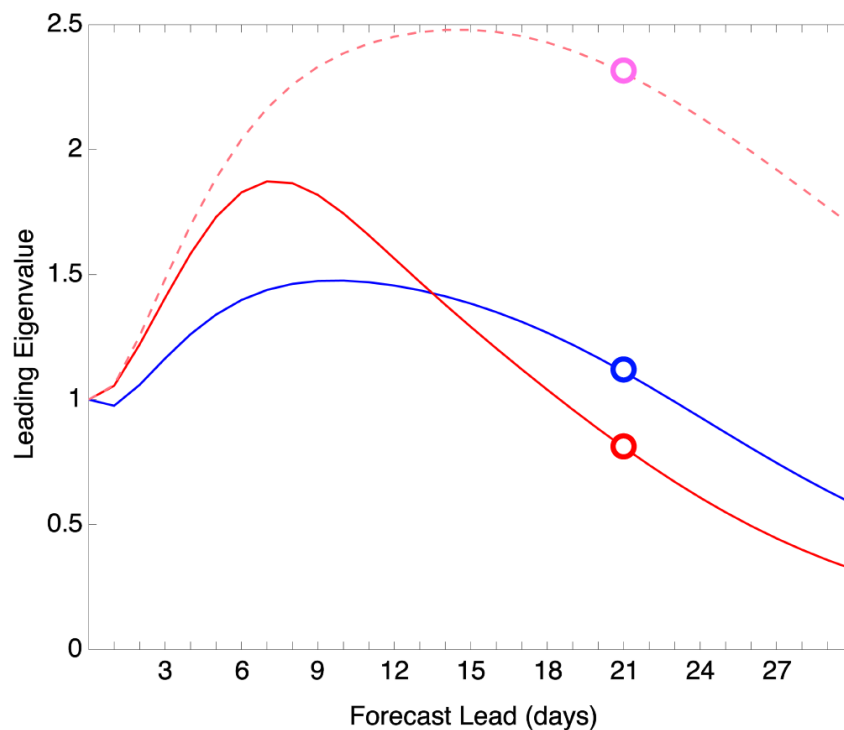
Figure 14. As Figure 12, but including blocking growth in the modified f-LIM (pink dashed line) that replaces 5 columns of the **L**-matrix with corresponding columns of the a-LIM, based on sensitivity tests from Figure 13.

The ability to capture NWP limitations in blocking prediction was also explored in Markov models, where the **G**-matrix is computed directly through lagged covariance. Climate Forecast System (CFS) reanalysis/reforecast data was used to produce the analysis-trained Markov model (A-MKV) and forecast-trained Markov model (C-MKV) for 1-4 week lead times, and the forecast performance for blocking was compared directly to the CFS NWP forecast (C-NWP). Correlation

of the blocking index in the forecast to verification demonstrates that C-NWP is superior to Markov models for 1-2 week lead times, but in weeks 3 and 4 the Markov model is superior (Fig. 15a); in addition, the Markov model trained on CFS forecasts decreases in skill at weeks 3 and 4 in a manner very similar to the CFS NWP forecast. This demonstrates that the empirical model trained on NWP model forecasts not only expresses reduced skill in blocking forecasts at subseasonal range, but the reduction in skill is commiserate with the reduction in skill of the NWP model forecast itself. This experiment shows that this technique is capable of retaining NWP model forecast deficiencies in a low-dimensional space where they can be investigated more easily.
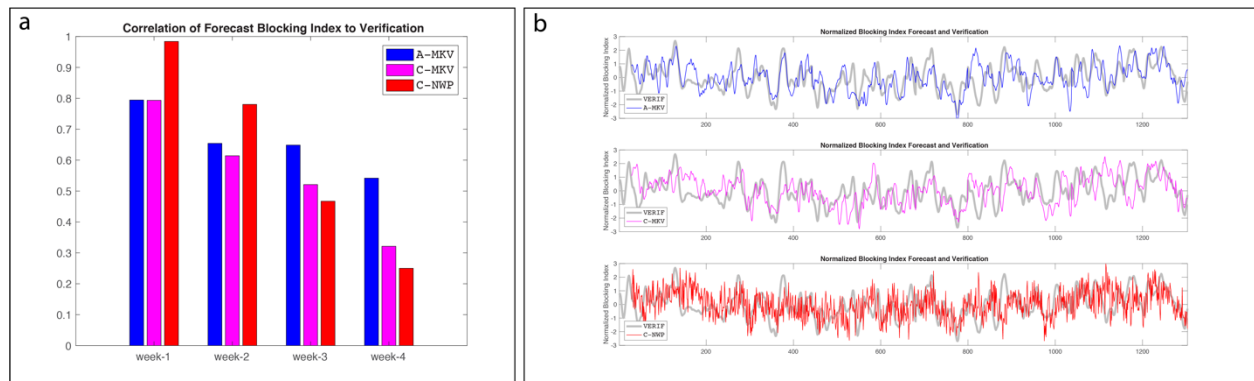
Figure 15. Correlation of the forecast blocking index with the verifying blocking index for forecasts with 1-4 week lead times from A-MKV (blue), C-MKV (magenta), and C-NWP (red). (b) Timeseries of the verifying blocking index (gray) with the week-4 forecast blocking index from A-MKV (blue, top), C-MKV (magenta, middle), and the C-NWP (red, bottom).

5. Conclusion

We have demonstrated that some aspects of challenges facing subseasonal range NWP can be contained within a drastically dimensionally-reduced space and inferred through linear modeling of atmospheric physics as expressed by both the real atmosphere (via reanalysis) and the NWP model (via reforecasts). Further, this can be achieved utilizing many of the same state variable components that are used in typical subseasonal forecast verification, requiring minimal additional reanalysis/reforecast data. These tools can be used to interrogate the differences between "real" physics and "model" physics, in the dimensionally-reduced space, to identify key interactions that are leading to reduced NWP skill at subseasonal ranges. This technique can also be applied to transition seamlessly from the week 1-2 NWP forecasting range to the week 3-4 subseasonal forecasting range, through utilizing the 5-day average NWP forecast as initial conditions for the linear inverse or Markov model. A forecast of this form would be able to take advantage of the near-range skill of the NWP model and the far-range skill of the empirical model.

6. Highlights of Accomplishments

- Development of 2-level/2-region streamfunction a-LIM, passing sanity tests
- Identification/development of blocking norm

- Development of LIM-derived optimal initial state for subseasonal-range growth of Pacific blocks
- Exploration of blocking growth in LIM separated into its midlatitude (streamfunction) and tropical (OLR) forcing components
- Development LIM formulation of GEFS-forecast driven low-dimensionality (LIM-like) forecast for investigating the role of model physics on subseasonal-range blocking forecasts
- Demonstration of a CFS-forecast driven Markov model retaining low skill in blocking forecasts at long (wk 3-4) range, similar to actual CFS model forecast
- Evaluation of differences in optimal initial structures and growth of blocks between CFS-forecast and analysis driven Markov models

7. Transitions to Applications

No transition to application at this time. A companion LIM has been developed in the Python programming language for use by the public.

8. Publications from the Project

Two papers have been published from this project in 2019:

Albers, J. R., and M. Newman, 2019: A priori identification of skillful extratropical subseasonal forecasts. *Geophysical Research Letters*, **46**, 12527-12536, doi: 10.1029/2019GL085270

Breeden, M.L., B.T. Hoover, M. Newman, and D.J. Vimont, 2020: Optimal North Pacific Blocking Precursors and Their Deterministic Subseasonal Evolution during Boreal Winter. *Monthly Weather Review,* **148**, 739–761, doi: 10.1175/MWR-D-19-0273.1

9. PI Contact Information

Contact the lead-PI through brett.hoover@noaa.gov

10. Budget for Coming Year

This is the final report for this project, there are no additional funds distributed in the coming year.

11. Future Work

This work constitutes the effort made on the entirety of the project.